M.S. Dissertation

Deflection-free Al_2O_3 membrane achieved by 2-step atomic layer deposition (ALD) technique

2-step 원자층 증착방법을 이용한 Al_2O_3 membrane의 표면 처짐현상 개선

BY

HYE JIN LIM

FEBRUARY 2017

DEPARTMENT OF MATERIALS SCIENCE AND ENGINEERING

COLLEGE OF ENGINEERING

SEOUL NATIONAL UNIVERSITY

Abstract

Deflection-free Al_2O_3 membrane achieved by 2-step atomic layer deposition (ALD) technique

With increasing attention paid to energy and environmental issues, LEDs have been intriguing replacements for traditional incandescent or fluorescent lights. Since the emergence of III-nitride family, GaN-based compound semiconductor grown on a sapphire substrate has been dominant in manufacturing a high-efficient LED device. However, obtaining a high quality GaN crystalline is a continuing technical challenge, which occurs due to the innate difference of material properties between sapphire substrate and GaN in hetero-epitaxy system. For example, there exists a large lattice mismatch between a sapphire substrate and GaN that results in reducing the light emission efficiency. Also, a higher refractive index of GaN compared to air prevents light from being extracted from the LED structure by provoking a total internal reflection and diminishes the light extraction efficiency. Furthermore, a substantial difference in the thermal expansion coefficients between sapphire and GaN film induces a wafer bow during the cooling process. The problem of wafer bowing restricts the fabrication of the device and hence decreases its productivity. Therefore, solving the aforementioned technical issues is of prime importance in enhancing the efficiency of LED chips.

Recently, our research group developed a groundbreaking growth scheme of GaN using cavity engineered sapphire substrate (CES) to achieve

high-efficiency GaN-based LEDs. In the CES scheme, GaN was grown on the crystalline α-Al_2O_3 membrane obtained by the phase transformations of amorphous-Al_2O_3. The amorphous-Al_2O_3 was deposited by atomic layer deposition (ALD) on a photoresist-patterned sapphire substrate and subsequently annealed at elevated temperature, forming the thermodynamically stable α-Al_2O_3. The annealed α-Al_2O_3, however, experienced a surface downward deflection during the phase transformation due to the volume contraction induced by a film densification, and this issue had a detrimental effect on the crystalline quality of GaN layer grown atop the annealed α-Al_2O membrane. The LED structure manufactured on the GaN template with poor crystalline quality, therefore, has lower internal quantum efficiency due to the generation of defects such as threading and misfit dislocations.

In this research, we investigated the density dependence of ALD Al_2O_3 film on its deposition temperature and addressed the effect of densified amorphous-Al_2O_3 on a degree of volume contraction after annealing. If the density difference between the amorphous-Al_2O_3 and α-Al_2O_3 during the phase transitions were minimized, the ensuing film was expected to have a reduced surface downward deflection accordingly. The ALD temperatures were varied ranging from 110 – 250 °C and the corresponding densities were measured by X-ray reflectivity (XRR). ALD deposition of amorphous-Al_2O_3 was carried out on a PR patterned sapphire substrate in a two-step process. Amorphous-Al_2O_3 was first deposited at 110°C for the thickness of 43nm to secure the pattern

shape and further deposited at various temperatures of 140, 170, 200 and 250°C for the rest of target thickness, 57nm. During the latter process, the deposition occurred at a higher temperature range to maximize the density of amorphous-Al_2O_3, aiming for the reduction in volume contraction as well as surface downward deflection upon thermal annealing. As a result, we observed the surface morphology of the annealed Al_2O_3 using atomic force microscopy (AFM) and found that the surface deflection was strongly dependent on the density of the ALD Al_2O_3 films. The specimen with amorphous-Al_2O_3 film deposited at 200°C during the second-ALD step demonstrated a 50% reduction in a surface deflection compared to the reference sample fabricated by conventional 1-step ALD. XRD result also exhibited the substantial improvement in crystalline quality of GaN (002) for this specimen due to the minimized surface deflection from volume reduction associated with the density increase.

Key Words:

Cavity engineered sapphire substrate (CES), 2-step atomic layer deposition (ALD), Phase transformation of Al_2O_3, Atomic force microscopy (AFM), X-ray reflectivity (XRR), Surface deflection

Student number: 2014-22531

Table of contents

List of Figures

Chapter 1. Introduction

1. Current issues with GaN-based LEDs

Light emitting diodes (LEDs) have been considered as promising substitutes for traditional incandescent light bulbs or fluorescent lighting due to their environmental-friendliness and low energy consumptions. A relatively high market price of LEDs, however, acts as a barrier to obtain wide acceptance among consumers although LED lighting companies strive to increase its global market share. According to the data provided by McKinsey's on global lighting market, the LED lighting business is expected to maintain a 3% annual growth rate until 2020 with its global market share reaching approximately 70% by then. Also, residential and architectural lighting sectors and outdoor lighting industry are forecast to grow apace in LED market [1].

A GaN-based compound semiconductor grown on a sapphire substrate has been dominantly used in manufacturing a power-efficient LED device. However, the inherent issues associated with the hetero-epitaxial dynamics between GaN and sapphire substrate remain as an important concern in manufacturing a high quality GaN film. For example, the large lattice mismatch between a sapphire substrate and GaN generates a high population of misfit and threading dislocations in the film and reduces the light emission efficiency accordingly. The difference in thermal expansion coefficient also induces a wafer bow, thereby not only impeding the use of large-diameter wafers but also reducing

the manufacturing productivity of GaN-based LED chips. Additionally, the amount of light extraction from the LED device is gradually reduced by the phenomenon of total internal reflection due to the large refractive index difference between air and GaN. Therefore, solving these issues is imperative to enhance the efficiency and device performance of LED structures [2].

1.1. Lattice mismatch and dislocations

A large lattice mismatch between a sapphire substrate (d = 2.748Å) and GaN film (d= 3.189Å) accounts for high threading and misfit dislocation density in the grown GaN film [3]. In GaN/Sapphire hetero-structures, the difference in lattice constants (~14%) generates missing or dangling bonds near the interface between the GaN film and underlying substrate, inducing the evolution of misfit dislocations thereafter. The prevailing dislocations serve as undesirable non-radiative recombination sites where electrons may be trapped in the deep defect levels and hence be unavailable to recombine with holes in active layer. A typical GaN film has a high threading dislocation density of 10^8 – 10^{10}cm^{-2} and a substantial reduction in dislocation density below 10^7 cm^{-2} is necessary to enhance the internal quantum efficiency of LED device as demonstrated in Figure 1.1 [4]. Despite the prevalence of populated dislocations in the grown GaN film, nitride material family is largely insensitive to dislocation defects compared to other types of III-V semiconductors such as GaAs. This insensitivity can be explained by compositional fluctuations in multi

quantum wells, which prevents the electrons from diffusing into the defect states by generating the localized valleys where electrons cannot escape due to their smaller diffusion length [5]. Threading and misfit dislocations in a GaN film are generally observed with cathode-luminescence or transmission electron microscopy as dark spots or lines.

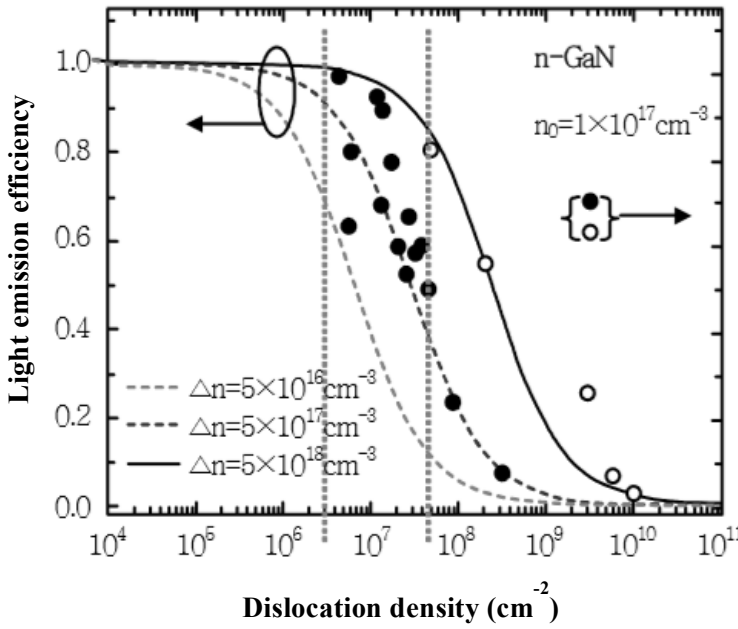

Figure 1.1 Light emission efficiency of n-GaN measured with respect to dislocation density (cm^{-2})

1.2. Thermal expansion coefficient mismatch

The thermal expansion coefficient of a-plane sapphire substrate is known as 7.50×10^{-6}/K at 300K while that of GaN layer is 5.59×10^{-6}/K resulting in a 36% mismatch [6]. During the cool-down process following the MOCVD growth of GaN film at 1040°C, the sapphire substrate with larger thermal expansion coefficient experiences thermal contraction with respect to the epitaxially grown GaN layer, thereby being susceptible to the tensile stress induced. Meanwhile, the GaN layer is affected by the compressive stress. In order to counteract this stress imbalance, the epitaxial wafer becomes elastically deformed into a convex shape. Therefore, the mismatch in thermal expansion between the sapphire and GaN epitaxial film is responsible for the appearance of a wafer bow, which has an adverse impact not only on crystalline quality of the grown GaN but also on fabrication productivity of GaN-based LED device. The problem of wafer bowing hinders large-scale mass production of GaN film, given that the degree of bowing deformation increases with increasing substrate diameter (in) as shown in Figure 1.2 [7].

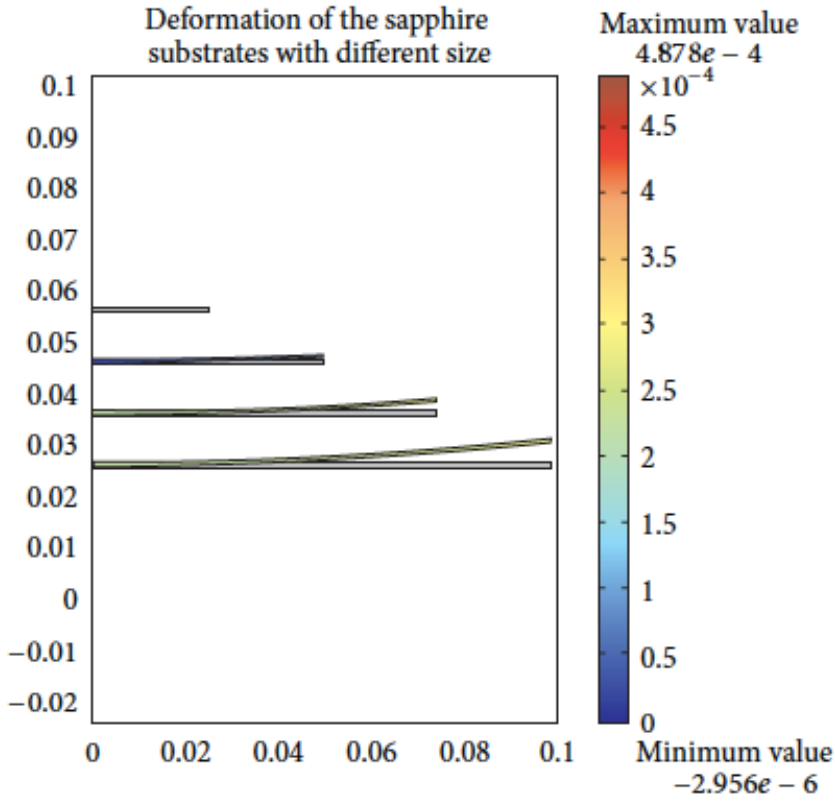

Figure 1.2 A degree of bowing deformation measured with increasing substrate diameter (in)

1.3. Refractive index difference

Higher refractive index of GaN ($n_{GaN} \approx 2.43$) compared to that of air ($n_{air} \approx 1$) and sapphires($n_{sapphire} \approx 1.7$) also leads to the diminished light extraction efficiency of LEDs [8]. The propagation of light waves from the GaN incident on an air is suppressed and reflected back to the first medium through the process known as total internal reflection. Based on the Snell's law, the phenomenon of total internal reflection occurs when the light from the medium with a higher optical density reaches the boundary at the incident angle greater than the critical angle (where the refraction angle becomes 90°). The light reflected becomes gradually absorbed within the GaN material until it vanishes entirely through the guided mode. Therefore, the abrupt change in refractive index prevents the light from being extracted from the LED device and results in inevitable reduction of the light extraction efficiency.

2. An overview of cavity-engineered sapphire substrate

Recently, our research group introduced a GaN-based LED grown on the air-cavity patterned sapphire substrate (CES) for enhancing the efficiency of LED chips as well as reducing the issue of wafer bowing [9]. In a CES scheme, micro-sized air cavity structures composed of amorphous-Al_2O_3 are embedded on a sapphire substrate. With the incorporated air-cavity patterns, it is expected to reduce the threading dislocation density via epitaxial lateral overgrowth (ELO) and lessen the degree of wafer bowing by 19% through the stress relaxation. In comparison with the patterned sapphire substrate (PSS) technique, the LED structure fabricated on CES demonstrated the enhanced optical output power by 39%, while remaining other technical advantages [10]. Most importantly, the dimensions, shape and the arrangement of the air-cavity patterns can be simply adjusted by modifying the photoresist patterns in CES system. In this paper, the contents regarding the striped-CES are to be addressed in the following sections.

2.1. Fabrication process of stripe-CES

The fabrication process of cavity-engineered sapphire substrate (CES) with stripe patterns is demonstrated in Figure 1.3 as a schematic diagram. First of all, a positive photoresist (PR), GXR 601, was distributed on a 2-inch sapphire substrate using MSX-1000 photolithography apparatus. The PR coated substrate was exposed to a UV light attached to EVG-620 mask aligner for making the desirable stripe patterns. The photo-masks for use in forming the stripes patterns

were prepared, with the pattern width of 3μm and 2μm respectively. The distance between the neighboring patterns were identical to 2μm for all occasions. The patterned PR was then placed in ICP etcher for 10 sec to descum the residual photoresist between the patterns. On top of the patterned structure, an amorphous-Al_2O_3 film was deposited by atomic layer deposition (ALD) for the target thickness of 100nm at 110°C. The underlying photoresist is stripped by acetone so as to obtain the thin amorphous-Al_2O_3 membrane with embedded cavities. Then, this amorphous structure is annealed in air-atmosphere furnace by two-stage thermal annealing at 850°C for 1hr plus 1150°C for 2hrs. During the thermal treatment, the remaining photoresist is completely removed by oxidation process and the amorphous-Al_2O_3 is fully crystallized into a single crystalline alpha-Al_2O_3 in order to achieve a thermodynamic stability. The corresponding alpha-Al_2O membrane becomes the template for the epitaxial growth of GaN film by MOCVD system.

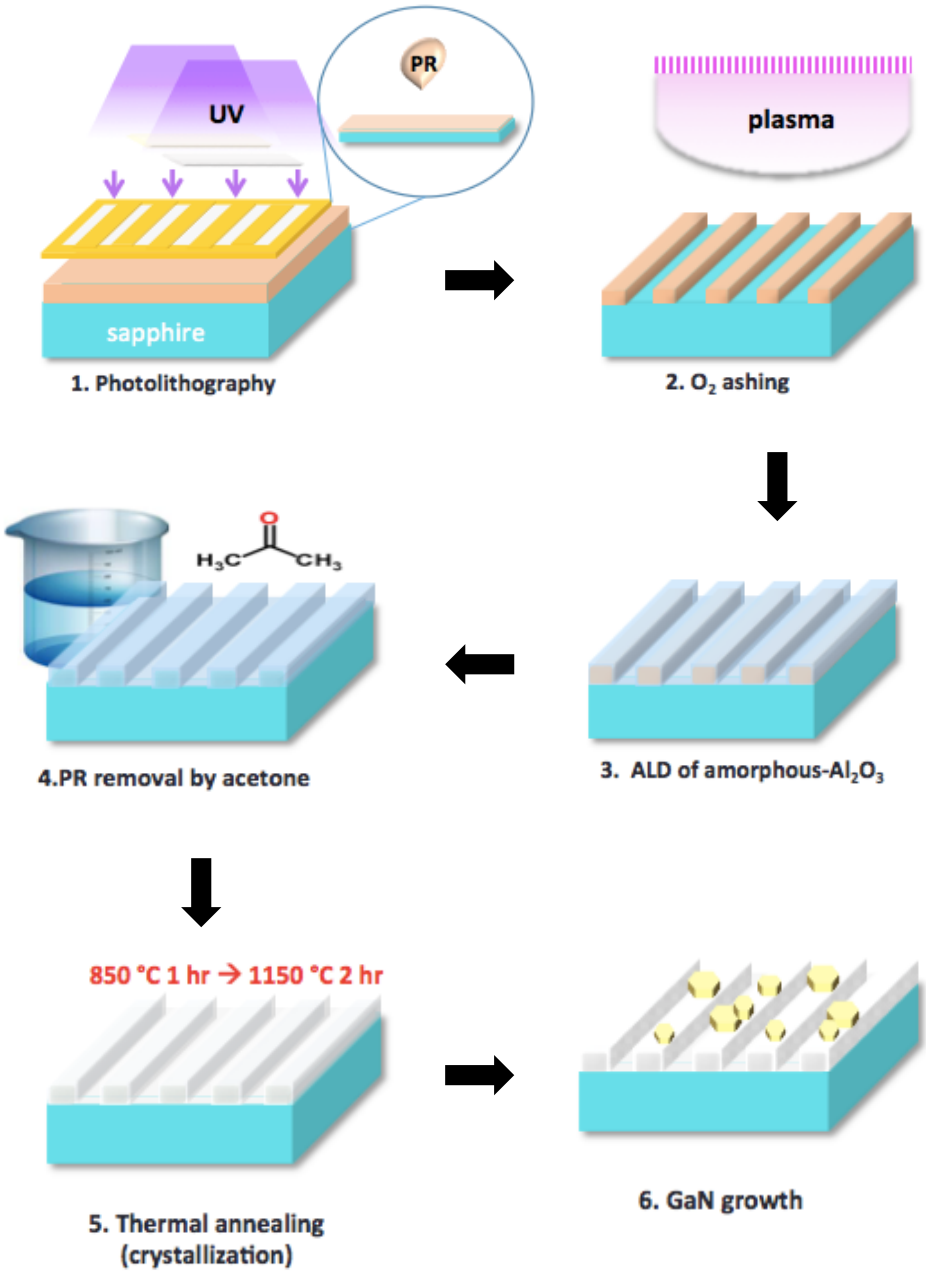

Figure 1.3 A schematic diagram of stripe-CES fabrication

2.2. Advantages and applications of stripe-CES

By manufacturing a thin layer of Al_2O_3 membrane as a substitution for sapphire, the effect of compliant substrate can be realized. The stress concentrated on a thin epitaxial film is substantially distributed to the substrate if the substrate becomes extremely thin as shown in Figure 1.4. With the increasing thickness ratio (h_{epi}/h_{sub}), the strain applied to the film reduces while that to the substrate increases [11]. Thus, the less-strained film becomes liberated from the strain-associated dislocations, which is highly desirable for the fabrication of power-efficient LED devices or defect-free thin film applications.

The sapphire substrate can be easily removed by mechanical lift-off if exerting a proper force on the fragile 100-nanometer thick Al_2O_3 membrane. As a dicing-less substrate, the stripe-CES contributes to the enhanced manufacturing productivity of GaN-based LEDs. Furthermore, the LED device fabricated on stripe-CES can be applicable to flexible GaN-based LEDs if transferred to flexible polymer substrates.

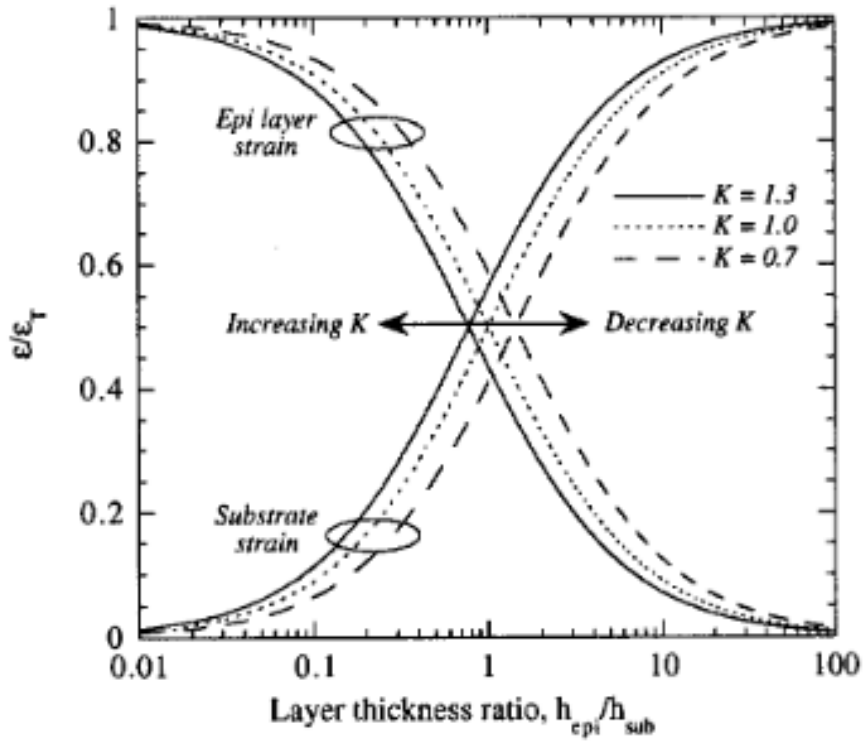

Figure 1.4 Strain partitioning between the epitaxial layer and underlying substrate in accordance with increasing thickness ratio (h_{epi}/h_{sub})

Chapter 2. Experimental tools

1. Film deposition technique

1.1. Atomic layer deposition (ALD)

Lucida D100 ALD system was employed to deposit a thin layer of amorphous-Al_2O_3 on a sapphire substrate, using Trimethylaluminum (TMA, $(CH_3)_3Al$) and water (H_2O) as aluminum and oxygen precursors, respectively. High purity nitrogen gas (N_2) of 99.9999% with the oxygen content less than 0.2ppm was used for the carrier gas in the reactor to remove the non-reacted precursors and gaseous by-products. Through the alternating exposure of TMA and water (0.2 sec for both TMA and water, 10 sec for a purge) at the growth temperature up to 300 °C, a highly conformal amorphous-Al_2O_3 layer was achieved. The film thickness can be easily controlled in angstrom precision by adjusting the number of cycles in ALD system.

1.2. Metal-organic chemical vapor deposition (MOCVD)

Tomas swan 3x2" close coupled showerhead (CCS) MOCVD system was used to obtain a GaN epitaxial layer. Trimethylgallium(TMGa,$(CH_3)_3Ga$) and Trimethylindium(TMIn, $(CH_3)_3In$) were entrained as the source precursors for Ga, and 99.9999% purified ammonia (NH_3) was used for N source. H_2 was used as a carrier gas. For the growth of p-GaN and n-GaN,

Bis(cyclopentadienyl)magnesium (Cp_2Mg, $(C_5H_5)_2Mg$) and diluted silane(SiH_4) with 10 ppm were used for p-type and n-type dopants, respectively.

2. Film characterization technique

2.1. X-ray reflectivity (XRR)

X-ray reflectivity technique was used as a metrological tool for analyzing the thin-film parameters of crystalline-Al_2O_3 membrane such as density, roughness, thickness and etc. The principle of XRR is based on the law of x-ray reflection. Provided that the x-ray beam strikes the film surface at the grazing angle (θ), the intensity of ray reflected off the surface or interface is measured by a detector rotating twice the incident angle (2θ). The beam is reflected at the surface and interfaces due to the difference in electron densities (i.e. refractive index) between the films.

If x-ray reaches the film surface at the angle above critical angle (θ_C), the incident x-rays penetrates into the films and a portion of x-rays becomes reflected at the interfaces or absorbed because of a large lattice spacing (d) between atoms according to the Bragg's reflection law of $n\lambda=2d\sin(\theta)$. The interference fringes propagated from the reflected x-ray is varied depending on the unique crystal structure of each material. Below the critical angle, on the other hand, the incident beam becomes totally reflected at the surface without penetration so that the intensity of reflection remains the maximum value of 1. Based on the intense study on the characteristics of x-ray reflection, thin-film

properties including film density, surface/interface roughness and thickness can be preferably obtained. Film density can be determined by the critical angle (θ_c) from the raw data where the intensity of reflectivity exhibits a dramatic reduction. The film with a higher density has a higher value of critical angle in degree as shown in Figure 2.1(a). Also, the distance of reflectivity oscillations indicates the layer thickness in a range of 0.1nm to 1000nm. A thicker film has smaller peak-to-peak distance of oscillations (Figure 2.1(b)). From XRR measurement, surface or interface roughness can be determined by the overall shape or gradient of oscillation graph. The prevalence of surface roughness decreases the reflected intensity by creating the diffuse scattering of the incident beam. Therefore, the film with a higher roughness demonstrated a steeper reflectivity line as in Figure 2.1(c). Amplitude of the thickness fringes provides the information regarding interface quality, roughness and resolution [12, 13].

PANalytical X'pert PRO equipment was used to take XRR measurement with an X-Ray Cu source operated at 40kV and 30mA. The instrument configuration is as follows. For incident beam optics, a divergence slit of 1/32 degree was employed. The reflectivity intensity with respect to the incident angle in degree was recorded from 0.001 to 2°. The step size for data collection was 0.002°. The smaller the step size is, the more accurate the obtained raw data by reflecting the minimal fluctuations. Remaining time per step size was 2 sec.

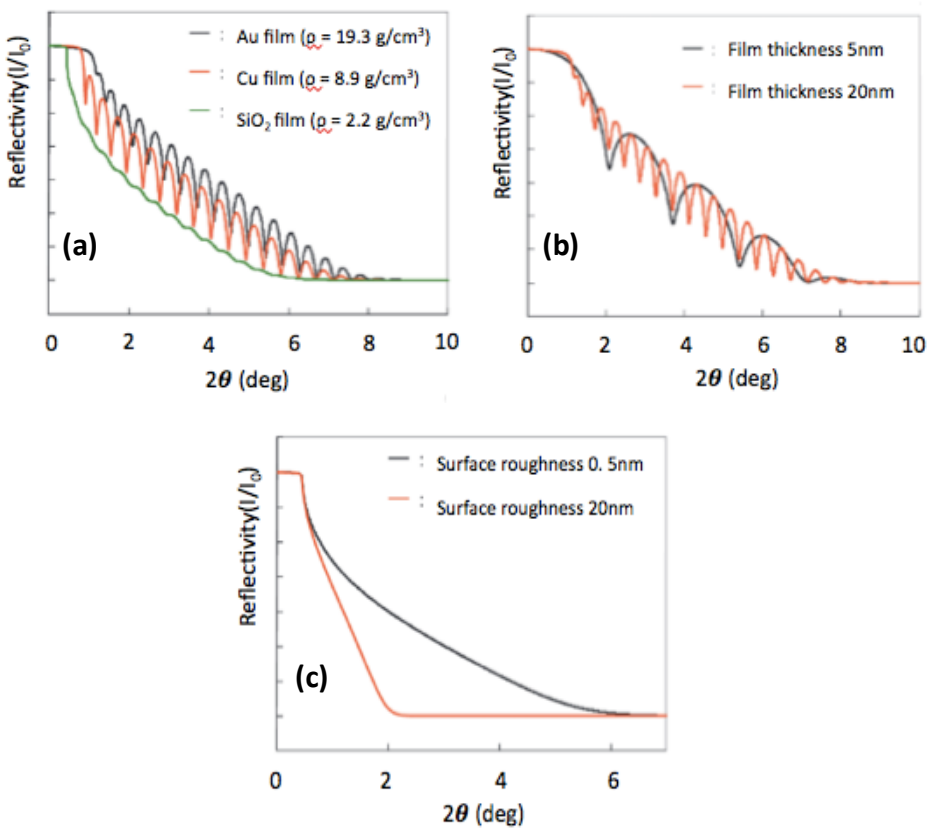

Figure 2.1 Effect of film (a) density, (b) thickness and (c) surface/interface roughness on X-ray reflectivity curve measured by XRR method

2.2. Atomic force microscopy (AFM)

Park Systems XE-100 was used as an analytical tool for film characterization of Al_2O_3 membrane. The basic principle behind its operation is that the attached probe (silicon SPM-sensor) detects the intermolecular force between the sample surface and itself to give information about surface topology. Surface morphology and roughness for Al_2O_3 were observed and analyzed with AFM in non-contact mode. XEI program was used as analysis tool for the obtained raw data.

2.3. Scanning electron microscopy (FE-SEM)

The surface morphology of Al_2O_3 membrane on stripe-CES was observed by a Hitachi S-4800 field emission scanning electron microscope (FESEM) operated at 15 kV. The dimensional properties of stripe-CES were preferentially analyzed with FE-SEM.

2.4. Transmission electron microscopy (TEM)

The Al_2O_3 membrane with embedded cavities in stripe-CES system was analyzed by transmission electron microscope (TEM), JEM-2100F, to observe the phase transformation-induced surface deformations after furnace annealing. TEM samples were prepared by using a focused ion beam (FIB) method.

Chapter 3. Phase transformation of Al_2O_3

1. Mechanism of phase transformations during annealing

1.1. Solid-phase-epitaxy (SPE) of Al_2O_3 in CES

During the thermal annealing process at the temperature 800 -1200°C, amorphous-Al_2O_3 experienced a series of phase transformations into a stable alpha-Al_2O_3 through solid phase epitaxy (SPE). During the phase transformations, Al_2O_3 goes through several intermediate phases such as delta and theta, whose occurrence cannot be guaranteed depending on the thermodynamic stability. The preferred phase transformation of Al_2O_3 from amorphous → gamma → alpha is summarized in Figure 3.1 as a schematic diagram. Provided that the phase transformation originated from the well-defined gamma/alpha interface toward the surface is maintained for a sufficient time at high temperature, according to Skald et al, amorphous-Al_2O_3 can be transformed into single crystalline alpha- Al_2O through solid phase epitaxy because phase transformation from gamma to alpha is proceeded in a much slower rate than that from amorphous to gamma [14, 15].

Amorphous- Al_2O_3 goes through two distinct steps of phase transformation as demonstrated in Figure 3.2. From amorphous to gamma phase transformation, the progression of single-crystalline gamma-Al_2O_3 toward the surface becomes obstructed by the formation of random nucleation cites prevalent, thereby inducing the polycrystalline phase to be evolved. Subsequently, the

polycrystalline gamma-Al_2O_3 is transformed into the single crystalline alpha phase through layer-by-layer phase transformation initiated from the bottom of the Al_2O_3 membrane.

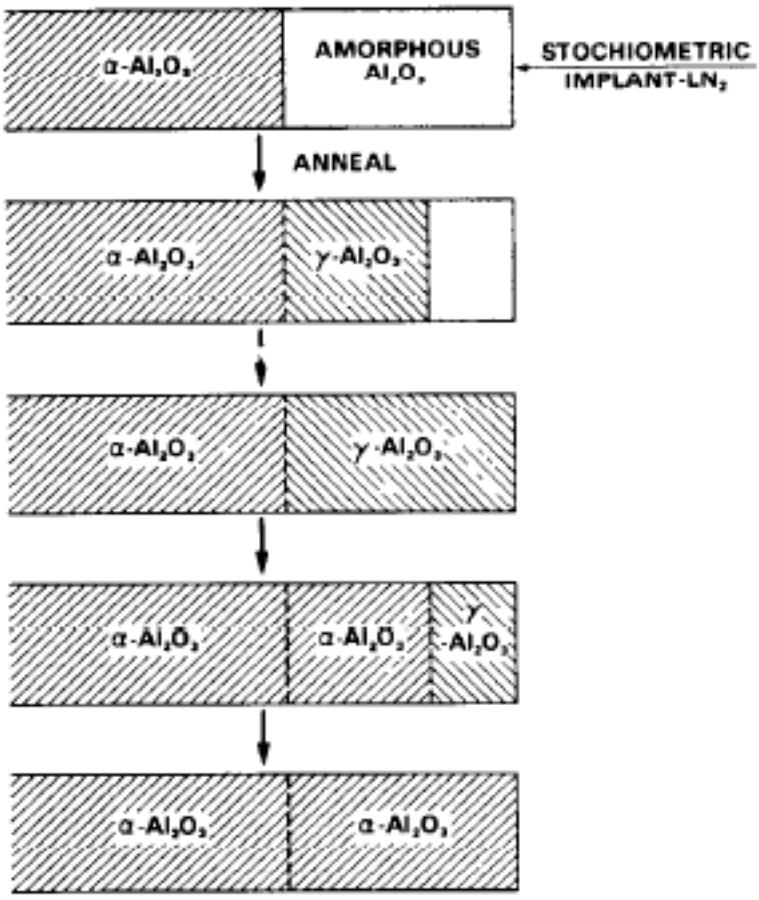

Figure 3.1 Phase transformations of amorphous-Al_2O_3 into alpha- Al_2O_3 by solid phase epitaxy [14]

1.2. Volume reduction of Al_2O_3 memb6ane

The density of amorphous-Al_2O_3 is 2.5-3.1 g/cm^3 depending on the ALD deposition temperature, and increases to 3.98 g/cm^3 for alpha-Al_2O_3 during the crystallization. The phase transformation-driven densification of the film leads to a drastic change in the volume and therefore provokes the structural deformation of the patterned membrane, which limits its functioning as a template for the growth of c-plane GaN.

During the amorphous to gamma phase transformation at the temperature of 850-900°C, the density of the membrane extensively increases to 3.65 g/cm^3 thus reducing its entire volume by 16 – 33% with the formation of polycrystalline-gamma phase. The gamma-Al_2O_3 is subsequently crystallized into alpha phase at the temperature above 1100°C through solid phase exitaxy, and the membrane suffers from the additional volume contraction. The further reduction in the volume intensifies the changes in surface morphology, causing a downward deflection to the patterned membrane surface due to the tensile stress induced as shown in Figure 3.2. The evolution of downward deflection along the patterned membrane surface and its mechanism behind will be discussed in the following section.

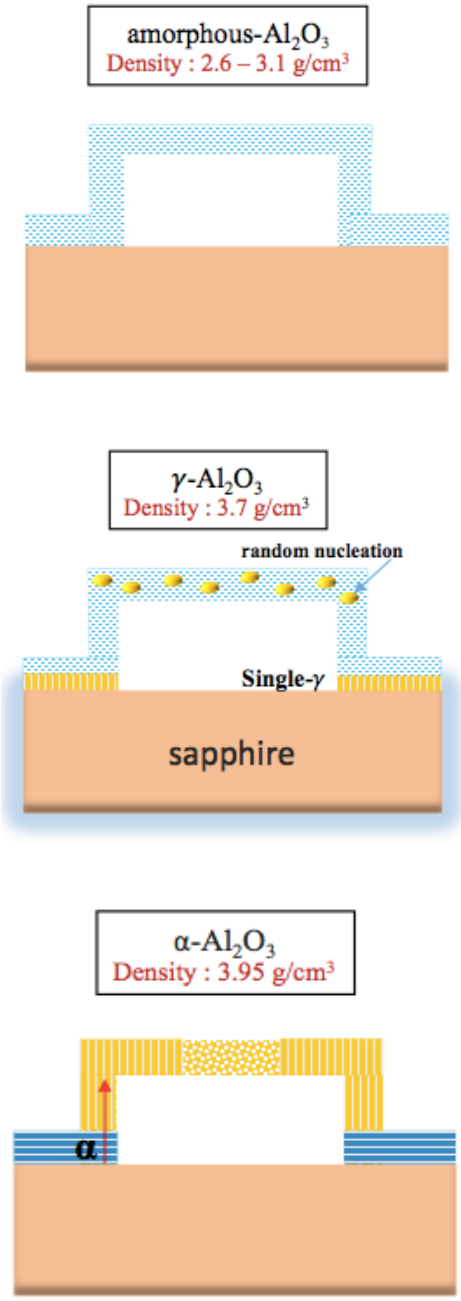

Figure 3.2 A schematic diagram of phase transition of patterned Al_2O_3 membrane in CES system

2. Problems of surface deflection in Al_2O_3-membrane.

2.1. Structural analysis of a surface deflection

During the phase transformations upon thermal annealing, the stripe-Al_2O_3 membrane undergoes a substantial volume contraction. The reduction in volume induces a surface deformation of the patterned membrane, modifying the membrane architecture against the original intent. While the entire membrane becomes contracted inward due to phase transformation-induced density increase, the angle (θ) between the membrane bridge and top surface constantly maintained even after annealing. Therefore, the membrane roof or surface becomes strained enough to provoke a surface deflection in order to achieve structural stability, inducing compressive stress to the inner surface of membrane bridge and tensile stress to the outer surface (Figure 3.3). The surface deflection depends on the following two parameters: membrane height and pattern width. If the width of patterned Al_2O_3 membrane increases, then a degree of surface deflection becomes intensified due to the increased portion of volume contraction. Therefore, it is desirable to shorten the pattern width to reduce the surface deflection thus achieving deflection-free membrane. Also, a degree of surface deflection increases with increasing pattern height. Compared to the Al_2O_3 membrane with a height of 2μm, the 3μm tall structure is expected to have reduced surface deflection due to the decreased angle between the membrane bridge and top surface.

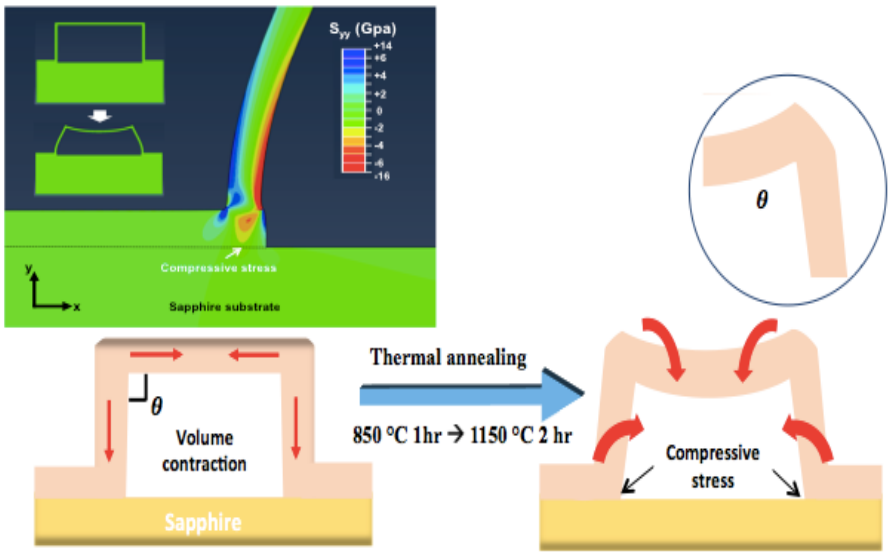

Figure 3.3 Structural analysis of surface deflection of Al_2O_3 membrane based on the simulation result.

2.2. Observation of surface deflection

The annealed α-Al_2O_3 was susceptible to volume contraction during the phase transitions that involved film densification, and this issue has a detrimental effect on the crystalline quality of the GaN film grown atop the densified α-Al_2O membrane creating the c-direction of GaN to be slanted. The LED structure manufactured on the GaN template with poor crystallinity, therefore, has lower internal quantum efficiency due to the formation of defects such as misfit and threading dislocations.

2.2.1. SEM image (3 μm x 2 μm)

A deflection of membrane surface upon thermal treatment was observed by field emission scanning electron microscope (FE-SEM). The SEM specimen was prepared by using the Al_2O_3 membrane with a pattern with of 3μm. The spacing between the patterns was 2μm. After annealing, the entire membrane experienced volume contraction as shown in Figure 3.4, thus causing the membrane roof to be deflected in convex shape. A degree of curvature increases as the distance away from the center point of the membrane roof increases.

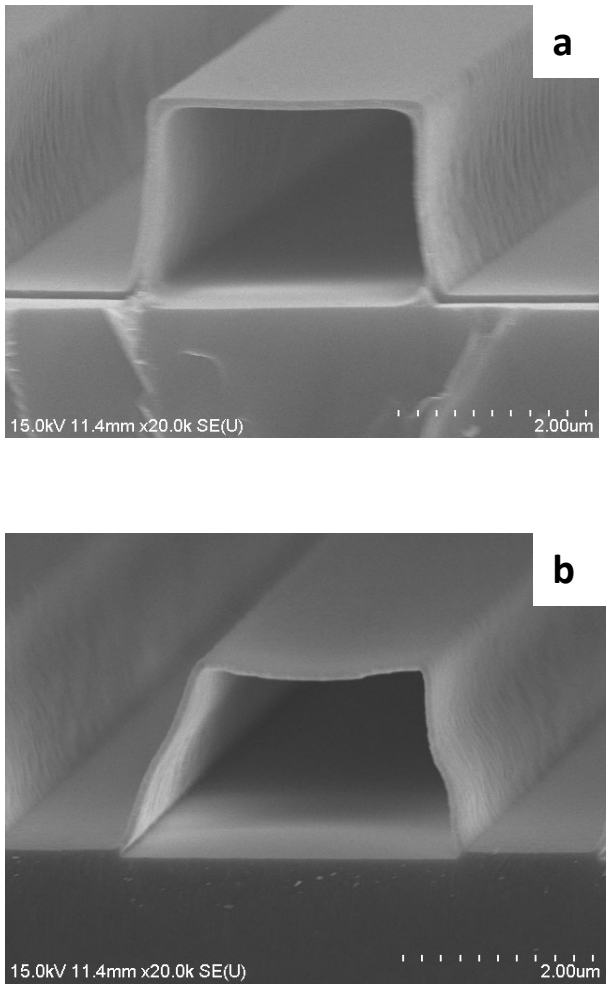

Figure 3.4 SEM images of Al_2O_3 membrane with a height of 3μm (a) before thermal annealing and (b) after annealing

2.2.2. AFM analysis

In order to measure a degree of deflection of Al_2O_3 membrane after annealing and investigating its surface morphology, atomic force microscopy (AFM) was utilized. Figure 3.5(a) and (b) denote that the membrane with 3μm pattern width has demonstrated a surface deflection of 100 nm from the imaginary horizontal line connecting the left and right ends of the pattern width. In case of the membrane with a pattern width of 2μm, a deflection of 60nm was measured. Based on this result, we once again confirmed that the deflection becomes more aggravated with increasing pattern width.

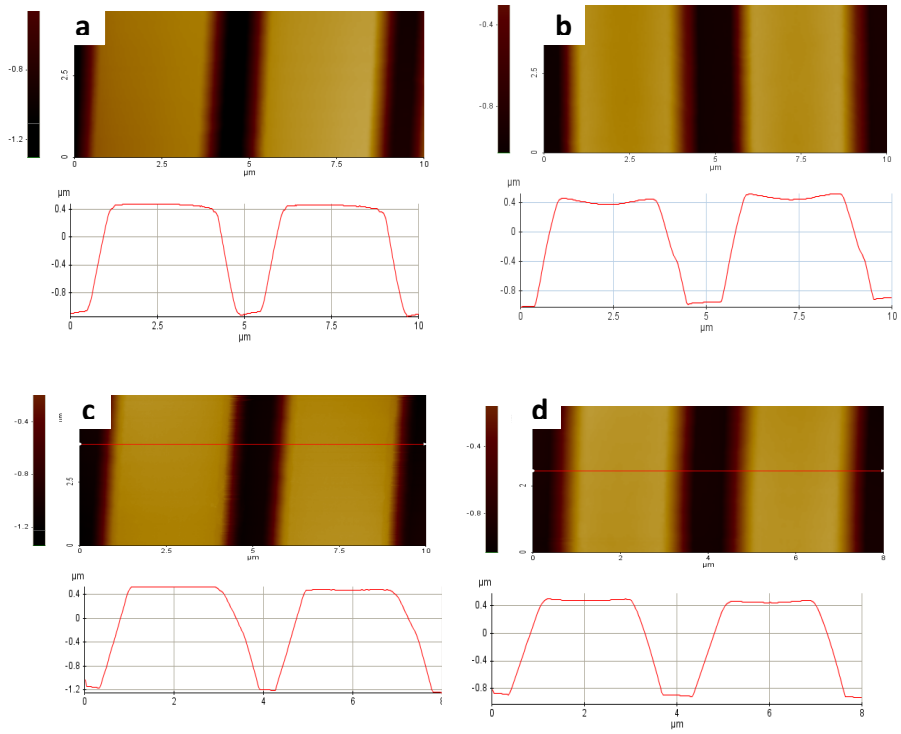

Figure 3.5 AFM images acquired to measure a degree of surface deflection along the Al_2O_3 membrane (a) as-annealed and (b) annealed for 3 µm x 2 µm stripe-CES and (c), (d) for 2 µm x 2 µm stripe-CES, respectively.

2.2.3. TEM analysis

A degree of surface deflection along the top surface of Al_2O_3 membrane was analyzed by TEM analysis. TEM images were acquired along a [11-20] zone, and the specimen was prepared with 2μm pattern-width Al_2O_3 membrane as a reference. TEM images and their diffraction patterns were taken at the left (counterclockwise) and right (clockwise) locations from a halfway point of Al_2O_3 membrane roof. The surface has demonstrated a deflection angle of ~ 2.3° with respect to c-axis of sapphire substrate, which is normal to the horizontal plane as shown in Figure 3.6. The growth of GaN on this deflected membrane inevitably leads to poor crystalline quality. Therefore it is of importance to reduce the surface deflection of the membrane induced by film densification.

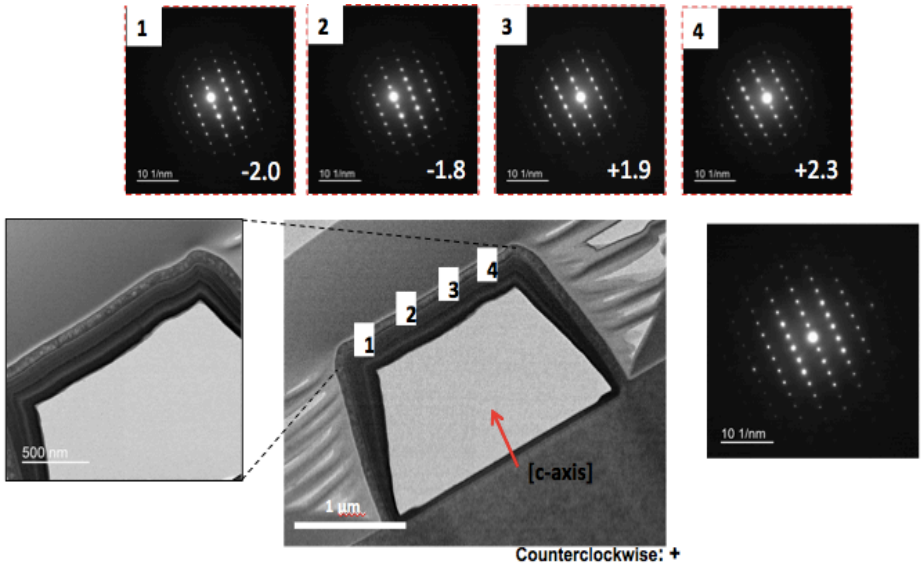

Figure 3.6 TEM image of Al_2O_3 membrane with 2µm pattern width to observe a degree of c-axis rotated along the top surface, with respect to the c-axis of sapphire substrate

Chapter 4. Two-step atomic layer deposition (ALD)

1. Reaction mechanism of ALD-Al_2O_3

Al_2O_3- thin layer fabricated with atomic layer deposition (ALD) has demonstrated precisely controlled film thickness and conformality. In general, ALD cycle is composed of the following four steps: metal-precursor exposure, purging, reactant exposure, purging. In case of amorphous-Al_2O_3 deposition, trimethylaluminum (TMA) and H_2O are used as metal precursor and oxidizing agent as Al and O sources, respectively. The precursors are alternately entrained to form Al_2O_3 film. When TMA precursor was first exposed to the sapphire substrate with a hydroxylated surface, aluminum atom from TMA reacts with the oxygen from hydroxyl (OH) group, forming a monolayer of Al-O-Al $(CH_3)_2$. Then, the excess TMA and CH_4 by-products are removed by a purging process with N_2 flow. Following the sufficient purging, H_2O vapor as an oxidation agent was exposed to remove the remaining CH_3 bonds, leaving the OH surface again. Finally, unreacted H_2O precursor and CH_4 by-products are evacuated by a further purging procedure. The schematic of ALD deposition of amorphous Al_2O_3 is illustrated in Figure 4.1. The above reactions can be summarized into the ensuing self-limiting reactions [16,17]:

(1) Al-OH + Al (CH_3) → Al-O-Al $(CH_3)_2$ + CH_4

(2) Al-CH_3 + H_2O → Al-OH + CH_4

Through the alternating pulse of TMA and H_2O at the optimum growth temperature, thin Al_2O_3 film with excellent step coverage can be obtained.

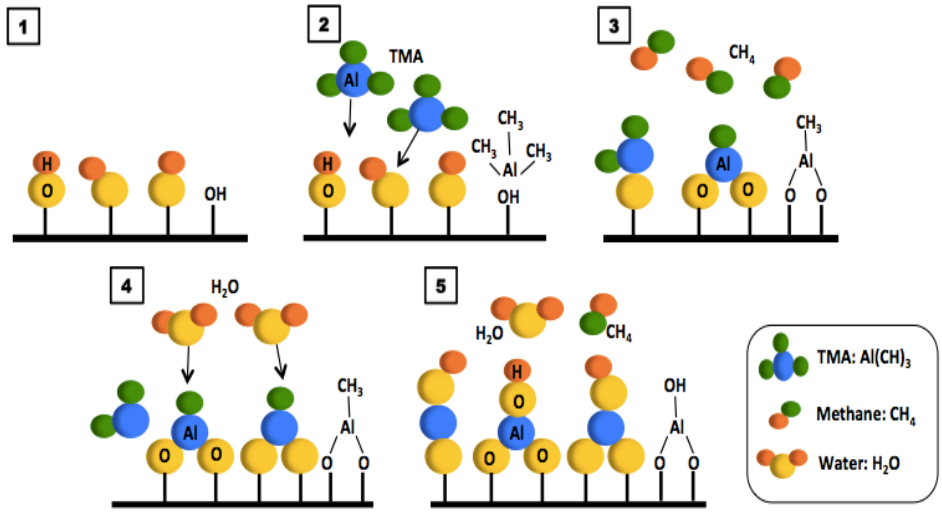

Figure 4.1 A schematic diagram of amorphous-Al_2O_3 film deposition by atomic layer deposition (ALD) using TMA and H_2O as precursors

2. Density of Amorphous-Al_2O_3 vs. ALD temperature

2.1. Analysis of density change with temperature

As denoted in many scientific studies, the density of ALD-amorphous Al_2O_3 becomes varied with respect to the growth temperature. That is, the density has demonstrated increasing tendency with increasing deposition temperature up to 200°C. At low temperature, the surface coverage of Al-OH group on sapphire substrate is high enough for active reaction sites. However, the thermal energy provided is insufficient to overcome thermal activation barrier, thereby preventing the completion of reaction. Thus, hydroxyl (OH) group becomes incorporated into the deposited Al_2O_3 film and serves as the impurities in film. Furthermore, H_2O has smaller desorption rate at lower temperature range (below 110°C). During the purging process, hydrogen atoms from H_2O reactant become trapped in the film as impurities in addition to hydroxyl group. As shown in Figure 4.2, the concentration of hydrogen atoms is higher at lower temperature and reduces with increasing deposition temperature [18]. Based on the aforementioned reasons, Al_2O film deposited at lower temperature has smaller film density compared to that grown at higher temperature. However, at temperature above 200°C, the entrained precursors become decomposed due to the lavish amount of heat energy provided thus reducing film density as well. Therefore, there exists optimum temperature range for ALD process.

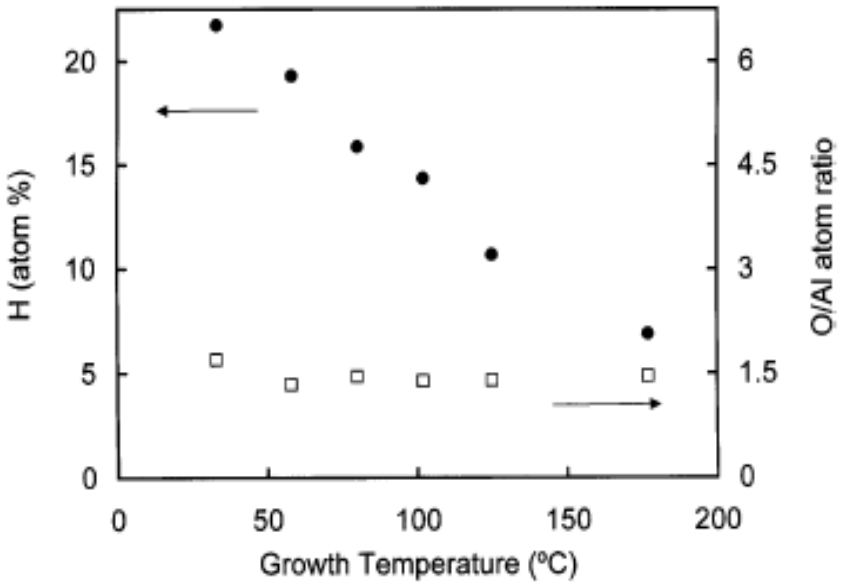

ALD property	Temperature(°C)		
	33	125	177
Density(g/cm^3)	2.5	2.95	3.0
%H-impurity	21.7	-	6.9

Figure 4.2 Level of hydrogen atoms (%) existing as impurities in Al_2O_3 film, varied with ALD growth temperature

2.2. X-ray reflectivity (XRR) for density measurement

2.2.1. Density determination from critical angle (θ_C)

From XRR measurement, the thin-film properties such as density, roughness and thickness can be analyzed. In this research, the primary aim for utilizing XRR technique is to determine the film density of amorphous-Al_2O_3, which has shown diversity with respect to the ALD deposition temperature.

The density of a film can be obtained by analyzing a critical angle of the recorded raw data of reflection intensity. From the reflectivity curve, the critical angle is defined as the point where the amount of light reflected decreases dramatically. The correlation between the film density and critical angle can be explained by the following equations, considering the unique property of x-rays. The refractive index (n) of x-rays is written as:

$$n = 1 - \delta - i\beta$$

where β indicates absorption effect and δ is dispersion. The absorption term can be ignored preferentially by assuming the free electron approximation. Therefore, the refractive index (n) can be reduced to

$$\mathrm{n} = 1 - \delta = \frac{\mathrm{r_e}}{2\pi}\lambda^2\rho_\mathrm{e} = \frac{\mathrm{r_e}}{2\pi}\lambda^2(\mathrm{Z}\cdot \mathrm{n_{atom}})$$

$$\mathrm{n_{atom}} = \frac{\mathrm{N_A}}{\mathrm{A}}\cdot\rho$$

where r_e = classical radius of the electron, λ = x-ray wavelength, μ = absorption coefficient, Z = number of electrons per atom, n_A = avogadro's number and ρ = density (g/cm^3)

By further applying the Snell's law, the correlation between film density and critical angle can be obtained by the following process:

$$1 - \delta = cos\theta \approx 1 - \frac{{\theta_c}^2}{2}$$

$${\theta_c}^2 \approx \sqrt{\frac{r_e}{\pi}\lambda^2\left(Z \cdot \frac{N_A}{A} \cdot \rho\right)}$$

Therefore, the density of a film, ρ, can be determined by the critical angle of reflection intensity curve [19].

2.2.2. Fitting procedure for XRR

In order to accurately analyze the film characterizations of Al_2O_3 layer, it is imperative to apply a fitting procedure for the obtained raw data. Through the fitting process, the collected raw data is compared with the simulated data by genetic algorithm. The preliminary simulation was processed based on the input variables regarding the thin layer and underlying substrate, such as expected roughness, thickness and density. After completing a fitting process, a fit-value, also known as chi-value, was obtained as an indicator of informing the reliability of fitted data. A fit-value is defined as the absolute value of the

difference between the intensities of each raw data and simulated data summed all over the points, which can be summarized as the following equation:

$$\text{Fit value} = \sum \left| \log I_{measured} - \log I_{simulated} \right|$$

A fit value closer to zero indicates a better prediction providing the data credibility. Since the fit index above 30 indicates a poor fit, the whole fitting procedure must be repeated until obtaining a best-fit value by continuously modifying the values of input parameters.

The Al_2O_3 film specimens prepared with all different ALD temperatures (110, 140, 170, 200, 250°C) were used to determine the film densities. For all occasions, a fit value below 30 was obtained for the data reliability. The fitted graph for the samples deposited at 110°C and 200°C were demonstrated in Figure 4.3, respectively. The red line indicates the simulated data and the blue line means the measured data. X'Pert Reflectivity was used as a fitting software and simulation was processed in the range of 0 to 1.2 degree to remove the adverse effects from intensity noises along the tail of the raw data curve.

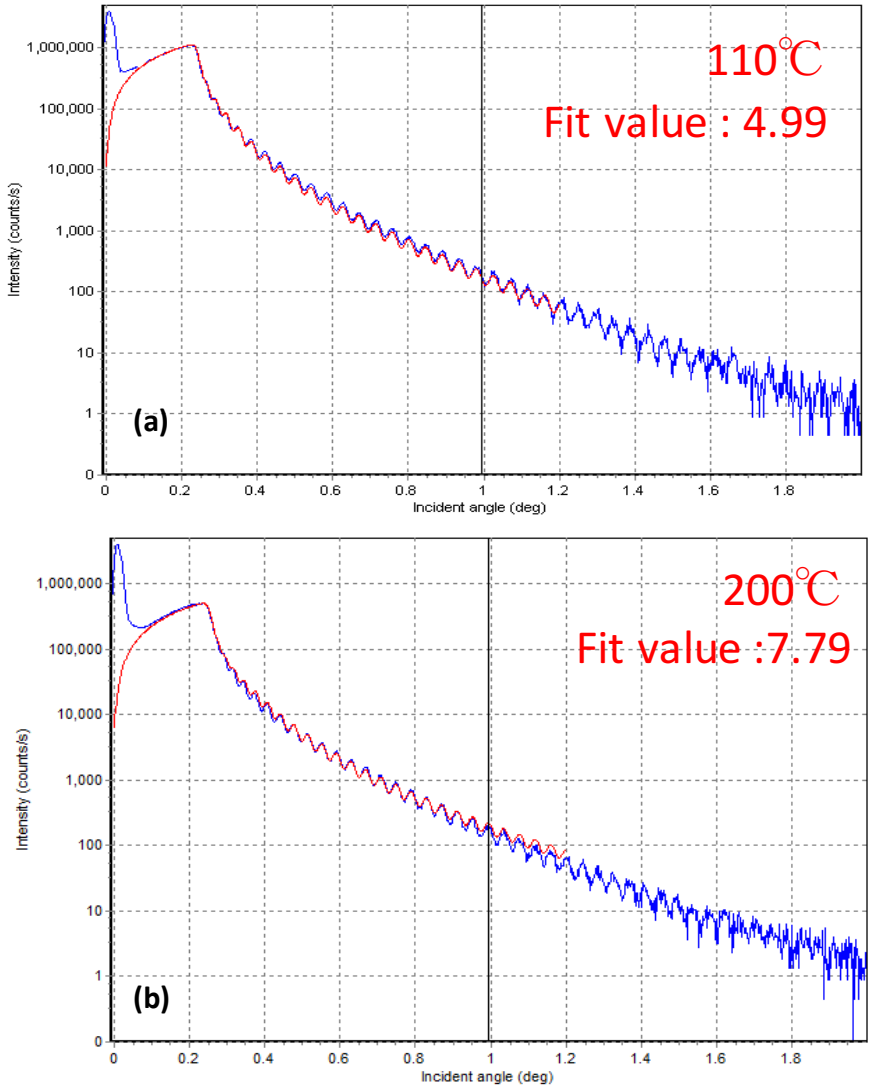

Figure 4.3 XRR reflectivity curves for the samples deposited at (a) 110°C and (b) 200°C during the second ALD step after a fitting procedure

2.2.3. Density of amorphous-Al_2O_3

The densities measured for amorphous-Al_2O_3 using X-ray reflectivity method are presented in the Figure 4.4. As shown in the graph, the density increases with the increasing ALD temperature up to 200C° and decreases afterward. The density was maximized at 200 C° as 3.158 g/cm^3 and minimized at 80C°. At a lower ALD deposition temperature range of ~ 110 C°, the film with very low density is manufactured due to the incorporated OH-group and H_2 impurities. At a higher temperature range above 200 C°, film density also becomes lower due to the prevalence of precursor decompositions by abundant thermal energy provided.

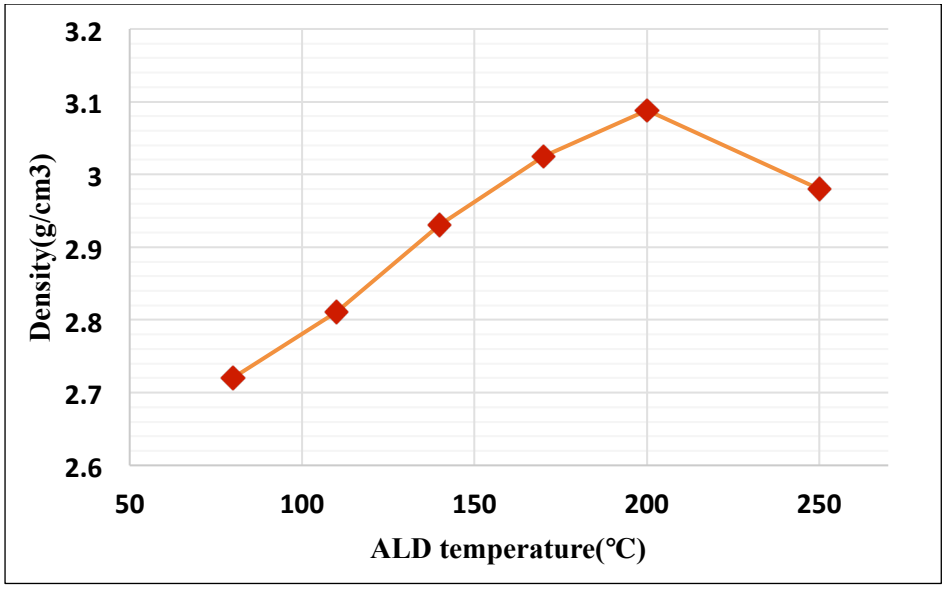

Tem.(C°)	80	110	140	170	200	250
Density(g/cm^3)	2.720	2.811	2.931	3.025	3.088	2.980

Figure 4.4 Density of amorphous-Al_2O_3 film with respect to ALD growth temperature ranging from 80 to 250°C, measured by XRR

3. Deposition of amorphous-Al_2O_3 by two-step ALD

3.1 Motivation of 2-step ALD

Al_2O_3 membrane suffers from the surface deflection after thermal annealing-induced phase transformations from amorphous to single-crystalline alpha phase. The observed deformation of membrane surface is hence associated with the volume contraction due to the density increase of 30 - 40%. Therefore, this work aims for reducing the surface deflection of the Al_2O_3 membrane by minimizing the difference in film density between amorphous and alpha-Al_2O_3. Reduction in a degree of surface deflection was attained through the two-step ALD deposition approach, based on the scientific premise that the density of amorphous-Al_2O_3 is varied depending on the ALD deposition temperature.

3.2 Fabrication process of 2-step ALD

As aforementioned, the density of amorphous-Al_2O_3 has exhibited an increasing tendency with increasing ALD deposition temperature up to 200°C. Since a downward deflection of the membrane surface occurs due to the density change during phase transformation, its substantial reduction can be achieved by the process called two-step ALD technique. In our previous work, we have deposited amorphous-Al_2O_3 membrane via single-step ALD process at 110°C instead of two separate steps. However, the amorphous film deposited at 110°C has a very low density of 2.720 g/cm^{3}compared to the values achievable at a higher ALD deposition temperature range. As a result, the two-step ALD

technique was developed to obtain the amorphous membrane with a higher density and hence minimize the density difference during the crystallization.

As the name implying, two-step ALD technique involves the deposition of amorphous-Al_2O_3 in two stages with respect to the deposition temperature – either high or low range – as demonstrated in Figure 4.5 as a schematic. The amorphous film is initially deposited at 110°C for 43nm thickness on a photoresist-patterned substrate in order to secure and stabilize the shape of the stripe patterns. 110°C is the maximum temperature where the underlying photoresist remains resistant to a thermal deformation during deposition. Then, the photoresist is subsequently removed by acetone and the specimen is rinsed with DI water in ultrasonicator for a cleaning. The film is further deposited at high-temperature range of 140-250 °C for the thickness of 57nm. The detailed experimental conditions (e.g. number of ALD cycles) will be discussed in the following section.

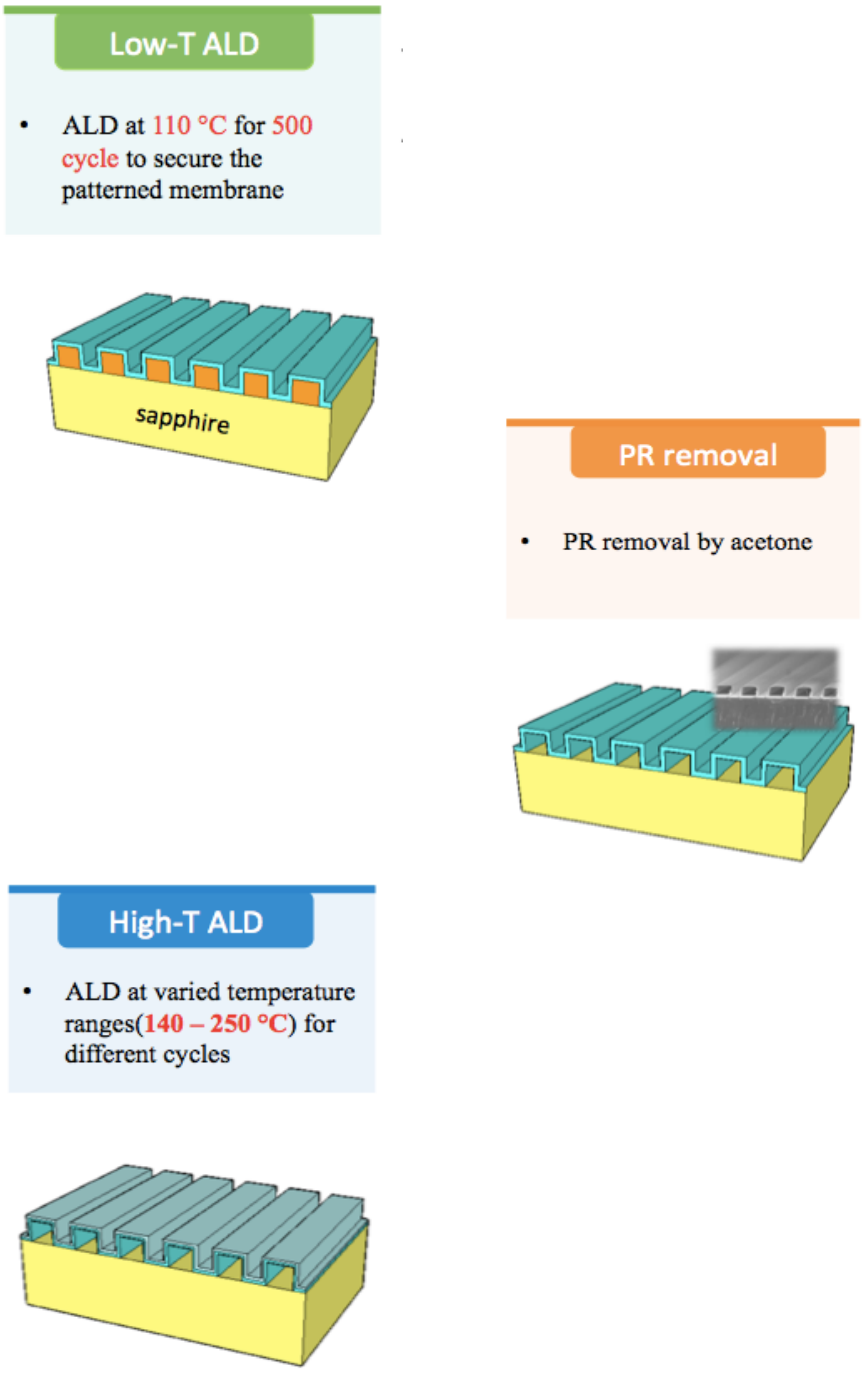

Figure 4.5 A schematic diagram of two-step atomic layer deposition

3.3 Experimental conditions

In order to obtain the thickness uniformity of 100 nm in two-step ALD process, the number of ALD deposition cycles for each temperature range was determined based on the film deposition rate (nm/cycle) in advance. Aamorphous-Al_2O_3 layer was deposited on a planar-Si(111) substrate at the temperature raning from 80 – 250°C for 300 cycles and the film deposition rate was determined by measuring the film thickness for each specimen. The thickness of the deposited amorphous-film was determined by Ellipsometer(Elli-SE-U) based on the law of reflection that depends upon the refractive index diffirence between the film and substrate. Therefore, Si(111) substrate was used as a substitution for sapphire substrate in this procedure because there is barely any diffference in refractive index(n) between amorphous-Al_2O_3 and sapphire(alpha-Al_2O_3). The value of film deposition rate was varied with increasing temperatures as summarized in Figure 4.6, with the maxium value of 0.1106 nm/cycle achieved at 200°C. Based on the calculated deposition rate for each temperature, the number of ALD cycles were determined for the second stage of two-step ALD process so that the otal thickness of Al_2O_3 membrane remained consistent for all occasions as 100 nm.

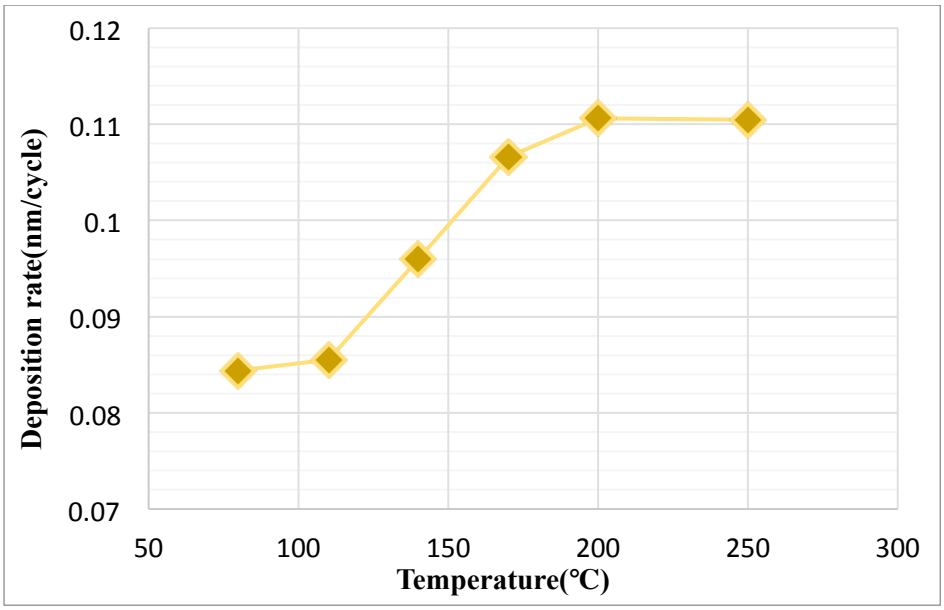

Tem.(C°)	80	110	140	170	200	250
Depo.rate (nm/cycle)	0.0844	0.0855	0.0960	0.1066	0.1106	0.1105

Tem. (C°)	110→140	110→170	110→200	110→250	110 (one-step)
# of cycle	500(43nm)				1200
	594 (57nm)	535	515	516	

Figure 4.6 A graph of deposition rate for Al_2O_3 film varied with increasing ALD growth temperatures.

Chapter 5. Effects of two-step ALD on reduction in surface deflection

1. Alpha-Al_2O_3 membrane with reduced surface deflection

1.1. AFM analysis

A degree of surface deflection on alpha-Al_2O_3 membrane after thermal annealing was analyzed by AFM technique. Compared to the stripe-CES fabricated with the conventional 1-step ALD method, the specimens prepared by 2-step ALD have demonstrated a reduced deflection along the membrane surface due to hindered volume contraction. Figure 4.7 exhibits the AFM images of stripe-CES fabricated with 2-step ALD method at various deposition temperatures before and after thermal annealing process. As shown in this figure, the top surface of Al_2O_3 membrane had not been deflected but remained flat for all occasions when as-annealed. Following the furnace annealing, the membrane experienced a shape deformation due to the phase-transformations and consequentially possessed a surface deflection along its surface. The degree of surface deflection was all varied depending on the ALD temperatures but minimized for the specimen with Al_2O_3 membrane deposited at 200°C, generating a 60% reduction compared to the reference sample fabricated by conventional 1-step ALD. It is assumed that the density of amorphous alumina was maximum when deposited at 200°C, thereby minimizing the density difference between amorphous phase and alpha phase.

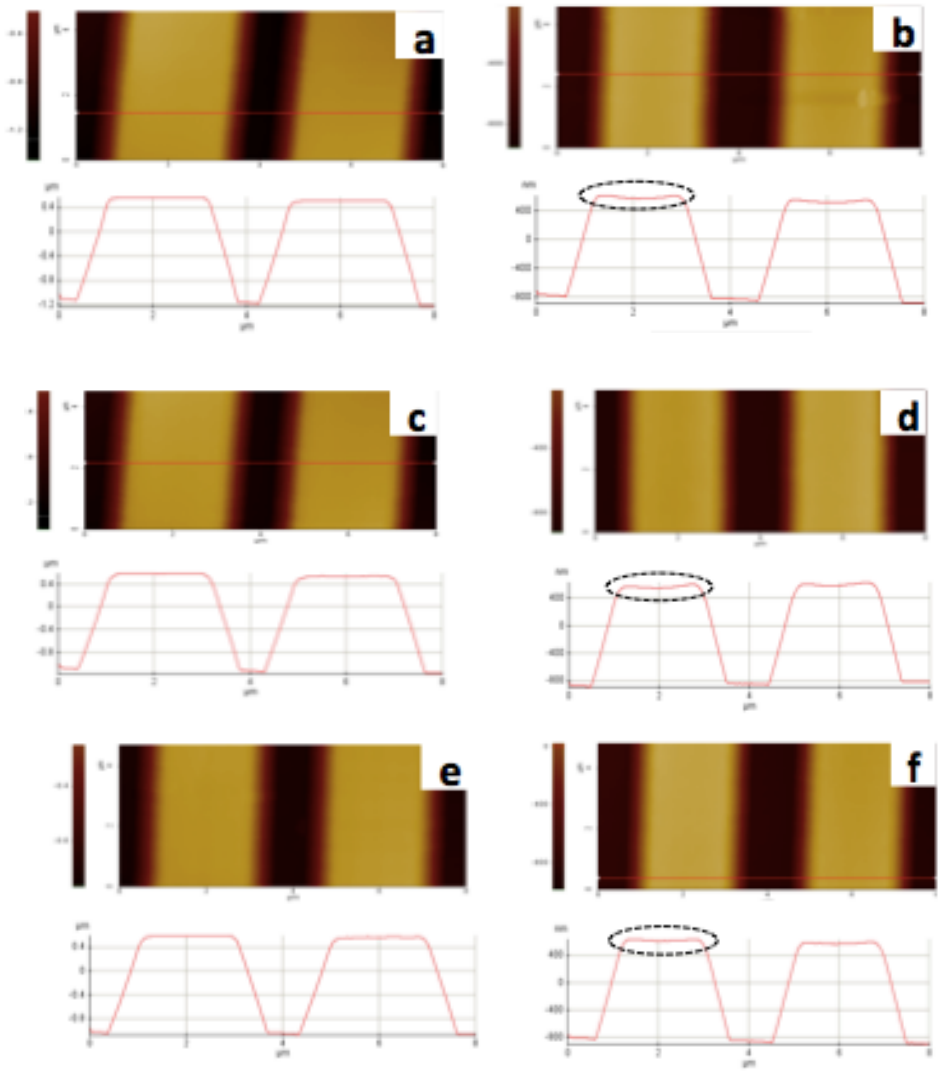

Figure 5.1 AFM images obtained to measure a degree of surface deflection along the Al_2O_3 membrane of 2μm x 2μm stripe CES (a) as-annealed and (b) annealed for 140°C, (b), (c) for 170°C, (d), (e) for 200°C and (f), (g) for 250°C respectively

1.2. TEM analysis

From TEM analysis, it was verified that the surface deflection of Al_2O_3 membrane was definitely reduced by applying the 2-step ALD technique. TEM images were acquired along a [11-20] zone, and the TEM specimen was prepared with 2μm pattern-width Al_2O_3 membrane. TEM images and their FFT patterns were taken at four different points from a halfway point of Al_2O_3 membrane roof. With the obtained diffraction patterns, the angle of deflection was calculated at each point with respect to the c-axis of sapphire substrate, which is normal to the horizontal plane. Compared to the reference sample with conventional 1-step ALD method, the specimen deposited at 200°C through 2-step ALD has demonstrated a reduced surface deflection angle of ~1.8° as shown in Figure 4.8. The issue of surface deflection was alleviated through 2-step ADL technique due to the diminished density difference between the initial amorphous and final single-crystalline alpha phase during the phase transformations.

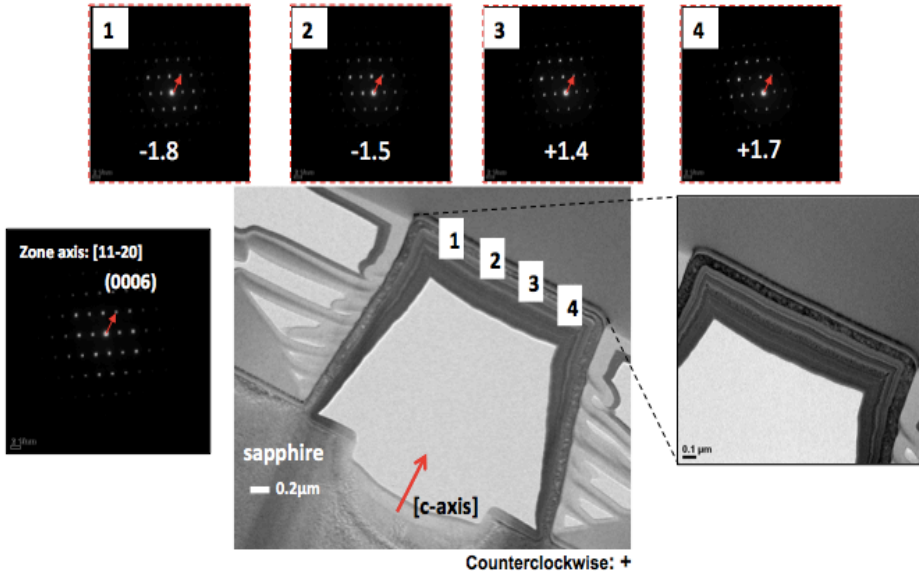

Figure 5.2 TEM image and corresponding diffraction patterns of Al_2O_3 membrane deposited at 200°C after applying 2-step ALD

2. GaN on alpha-Al_2O_3 with reduced surface deflection

1.1 XRD measurement compared to reference

The crystalline quality of GaN layer grown on alpha-Al_2O_3 membrane was analyzed by X-ray diffraction method to observe the interaction between the reduced surface deflection and ensuing improvement in crystal quality when applying the 2-step ALD. GaN was grown by MOCVD at 1040°C for 90 min. Since the deflection along the membrane roof has been the fundamental cause for the c-axis tilt in GaN relative to the substrate normal, we measured the XRD rocking curves of GaN (002) and GaN (102) planes and obtained the corresponding values of FWHM. Compared to the reference sample, GaN layer on the Al_2O_3 membrane deposited at 200°C by 2-step ALD has exhibited smaller FWHM value of 583 arcsec for GaN(102) plane, giving a 27% reduction. The substantial improvement in the crystalline quality of GaN layer is thought to be due to the reduced surface deflection as a result of minimized density difference during the sequential phase transformations.

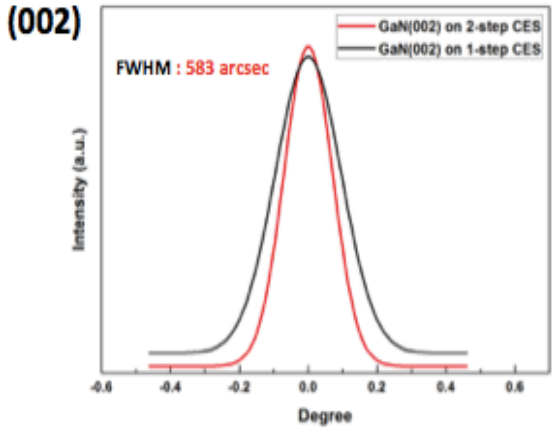

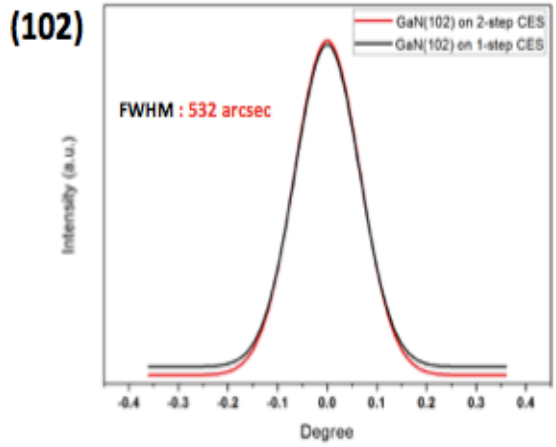

Tem.(°C)	(002)	(102)
1-step(ref.)	803 arcsec	536 arcsec
140	724	561
170	673	532
200	583	558
250	1000	800

Figure 5.3 FWHM values of GaN(002) and GaN(102) peaks for the GaN layer grown on Al_2O_3 membrane fabricated with 2-step ALD technique

Conclusion

This work concentrates on investigating the film-densification and volume contraction of Al_2O_3 membrane and ensuing surface deflection issue during the annealing-induced phase transformations. During the thermal treatment, amorphous-Al_2O_3 membrane undergoes a series of phase transitions into a stable alpha-Al_2O_3 through solid phase epitaxy, involving the increase in film density and surface downward deflection due to the volume contraction. Therefore, the ultimate purpose of this research is to reduce the surface deflection of Al_2O_3 membrane by minimizing the density difference between the amorphous-Al_2O_3 and crystalline α- Al_2O_3 through the variation of ALD deposition temperature known as two-step atomic layer deposition technique.

Reference

[1] Mckinsey&Company, Lighting the Way*:* Perspectives on the Global Lighting Market (2nd Edition), *5-37 (2012)*

[2] F. K. Yam, L. L. Low, S. A. Oh, and Z. Hassan, Gallium Nitride: An Overview of Structural Defects, Optoelectronics, Materials and Techniques, 109 (2011)

[3] D. Zhu, D. J. Wallis and C. J. Humphreys, Prospects of III-nitride optoelectronics grown on Si, Rep. Prog. Phys. 76, 106501 (2013)

[4] Light Emitting Diodes (LEDs) for Generating Illumination," OIDA Technology Road MapUpdate 2002, (2002)

[5] E. Fred Schubert, Light-Emitting Diodes (Second edition), New york: Cambridge University Press, 123-126 (2006)

[6] L. Zhang et al, Influence of stress in GaN crystals grown by HVPE on MOCVD-GaN/6H-SiC, Scientific Reports 4, 4179 (2014)

[7] W. Bin, Q. Yu-xuan, H. Shi-gang, T. Zhi-jun, L. Jin, and H. Ying-lu, Simulation and Analysis of GaN Wafer Bowing on Sapphire Substrate, Advances in Condensed Matter Physics. 2013, 2-3 (2013)

[8] E. Ejder, Phys. Status Solidi (*a)* 6, 445-448 (1971)

[9] J. Jang et al**.** Incorporation of air-cavity into sapphire substrate and its effect on GaN growth and optical properties, J. Crystal Growth. 45, 430 (2015)

[10] Moon et al, Microstructured Air Cavities as High-Index-Contrast Substrates with Strong Diffraction for Light-Emitting Diodes, Nano Letters. 16, 3301- 3308 (2016)

[11] D. Zubia and S. D. Hersee, The heteroepitaxy of mismatched semiconductor materials, Journal of Applied Physics. 85, 6492 (1999)

[12] M. Sardela, X-ray analysis methods, Advance Materials Characterization Workshop (2008).

[13] M. Yasaka, X-ray thin-film measurement techniques, Rigaku J. 26 (2), 1-9 (2010).

[14] C.W. White et al., Ion implantation of crystalline oxides and ceramics, Nuclear Instruments and Methods in Physics Research B 32, 11-22 (1988)

[15] P.S. Sklad, J.C. McCallum, C.J. McHargue, and C.W. White, The amorphous-to-gamma transformation in ion implanted Al_2O_3, Nuclear Instruments and Methods in Physics Research B 46, 102-106 (1990)

[16] A.W. Ott, J.W. Klaus, J.M. Johnson, and S.M. George, Al_2O_3 thin film growth on Si (100) using binary reaction sequence chemistry, Thin Solid Films 292, 135-144 (1997)

[17] S.K. Kim, S.W. Lee, and C.S. Hwang, Low Temperature (<100°C) Deposition of Aluminum Oxide Thin Films by ALD with O 3 as Oxidant, Journal of The Electrochemical Society 153 (5), F69-F76 (2006)

[18] M. D. Groner, F. H. Fabreguette, J. W. Elam, and S. M. George, Low-Temperature Al2O3 Atomic Layer Deposition, Chem. Mater. 16, 639-645 (2104*)*

[19] J. A.Bokhoven and C. Lamberti, X-ray absorption and X-ray emission spectroscopy: Theory and applications. Chichester, West Sussex: John Wiley & Sons, 254-255 (2015)

국문초록

GaN 기반 LED는 기존의 백열등, 형광등보다 우수한 에너지 효율과 긴 발광 수명으로 인해 차세대 조명 기술로 각광받고 있다. 일반적으로 LED chip을 제작하기 위해서 GaN기반 화합물 반도체를 사파이어 기판 위에 epitaxial 하게 성장시킨다. LED의 발광 효율을 향상시키기 위해 사파이어 기판의 표면을 가공하여 난반사를 높이는 연구가 활발하게 진행되고 있으며, 우리 실험실 에서도 최근 cavity engineered sapphire substrate(CES)를 개발해 연구를 진행하고 있다. CES 기판 위에서 GaN 박막을 성장시킬 경우 lateral overgrowth가 일어나 관통 전위 밀도가 감소하게 되며 air-cavity 패턴들에 의한 난반사로 인해 광 추출 효율이 증가하게 된다. 또한 기판과 GaN박막 사이에 존재하는 cavity 구조에 의해 GaN 박막 내부의 응력이 줄어 기판의 휨 현상도 완화되며, 이는 LED 소자 공정의 생산성을 크게 증가시킨다. Photoresist(PR)를 이용하여 원하는 형태, 크기, 분포의 air-cavity 패턴을 만들 수 있으며 이를 통제하여 최적 조건의 기판을 제작할 수 있다는 장점이 있다.

고온 열처리 과정에서 amorphous-Al_2O_3 는 solid phase epitaxy를 통해 기판과 같은 상태인 단결정의 alpha-Al_2O_3로 상 변화하게 된다. amorphous-Al_2O_3의 밀도는 ALD 공정 온도에 따라서 달라지게 되지만 보통 2.4 ~ 3.0 g/cm3이며, alpha-Al_2O_3의 경우 밀도는 3.95로 고정된 값을 가진다. 열처리 과정에서 박막의 상태

변화로 인해 약 15% 정도의 밀도 증가현상이 일어나고 이로 인해 부피가 감소하게 되어 박막의 표면이 아래로 쳐지는 deflection현상 및 표면의 거칠기가 증가하는 문제점이 발생하게 된다. 패턴 표면의 거칠기가 심화되거나, deflection이 발생하게 되면 그 위에 성장되는 GaN 표면의 c-plane이 틀어지게 되어 결정성에 악영향을 미치며, 결과적으로 그 위에 성장되는 LED구조의 효율이 저하된다. 그러므로, 패턴 표면의 deflection 및 거칠기 문제를 해결하는 것이 매우 중요하다. 따라서 본 논문에서는 2-step ALD 공정을 이용하여 앞서 언급된 문제를 해결하고자 하였다. 2-step ALD 공정은 저온 증착과 고온 증착 두 단계로 이루어진다. 저온 증착 단계에서는 패턴의 모양을 유지시키기 위해 PR의 변형이 일어나지 않는 최대 온도인 110도에서 공정을 진행한다. 고온 증착 단계에서는 amorphous-Al_2O_3와 alpha-Al_2O_3의 밀도 차이를 최소화 시켜 표면의 거칠기와 deflection을 감소시키기 위해 높은 밀도의 amorphous-Al_2O_3를 증착 할 수 있는 온도에서 공정을 진행한다. Amorphous-Al_2O_3 경우 ALD 공정 온도에 따라 밀도가 달라지게 된다. 낮은 온도(80~140℃)의 경우, 박막 증착을 위해 이용되는 precursor들의 desorption rate이 낮아 –OH기같은 불순물이 생성되기 때문에 증착된 Amorphous-Al_2O_3 박막의 밀도가 낮아지게 된다. 따라서 ALD 공정 온도가 높아질수록 증착된 박막의 밀도가 증가하지만 또한 너무 높은 온도(>250℃)에서는 과도한 thermal energy가 공급되어 precursor의 분해가 일어나Amorphous-Al_2O_3의 증착이 제대로 이루어지지 않아 밀도가 낮아지게 된다. 따라서

고온 증착 단계의 온도를 140~250℃ 사이의 값으로 변수를 주어 표면의 거칠기와 deflection을 최소화 시키는 온도를 찾는 것이 이연구의 목표이다.

주요어:

Cavity engineered sapphire substrate (CES), 2-step ALD 공정, Al_2O_3의 상변화, 표면 deflection, Atomic force microscopy (AFM), X-ray reflectivity (XRR)

Student number: 2014-22531